# Articles

# Observational Constraints on the Global Atmospheric CO₂ Budget

PIETER P. TANS, INEZ Y. FUNG, TARO TAKAHASHI

Observed atmospheric concentrations of $CO_2$ and data on the partial pressures of $CO_2$ in surface ocean waters are combined to identify globally significant sources and sinks of $CO_2$. The atmospheric data are compared with boundary layer concentrations calculated with the transport fields generated by a general circulation model (GCM) for specified source-sink distributions. In the model the observed north-south atmospheric concentration gradient can be maintained only if sinks for $CO_2$ are greater in the Northern than in the Southern Hemisphere. The observed differences between the partial pressure of $CO_2$ in the surface waters of the Northern Hemisphere and the atmosphere are too small for the oceans to be the major sink of fossil fuel $CO_2$. Therefore, a large amount of the $CO_2$ is apparently absorbed on the continents by terrestrial ecosystems.

RISING ATMOSPHERIC $CO_2$ CONCENTRATIONS ARE EXPECTed to lead to significant global climatic changes during the coming decades (1). After 30 years of measurements in the atmosphere and the oceans, the global atmospheric $CO_2$ budget is still surprisingly uncertain. An improved understanding of the $CO_2$ cycle is essential to predict the future rate of atmospheric $CO_2$ increase and to plan eventually for an international $CO_2$ management strategy.

Combustion of fossil fuels, the amount of which is well documented (2), is a major contributor to the observed concentration increase of $CO_2$ in the atmosphere. The measured rise was about 57% of the fossil fuel input from 1981 to 1987. Other sources may have also contributed to the rise, but the amount of $CO_2$ released by changes in land use remains uncertain (3, 4), as is the response of terrestrial ecosystems to higher $CO_2$ levels and to other climatic and environmental perturbations (5). Estimates of the uptake of $CO_2$ by the oceans have been based entirely on computational schemes of varying complexity (6), from "box" models to three-dimensional ocean circulation models (7). The "consensus" among these studies is that the oceans might be absorbing between 26 and 44% of the fossil $CO_2$. This would leave no room for any significant net loss of C from terrestrial ecosystems, but instead would require net C

uptake on the land (except for the highest ocean uptake estimates) to balance the atmospheric $CO_2$ budget (6, 7).

The inorganic carbon chemistry that describes the ultimate uptake capacity of the oceans is well understood; however, the capacity of the oceans for uptake of $CO_2$ also depends sensitively on their circulation dynamics and the biological processes in them. The atmosphere exchanges $CO_2$ with the ocean surface layer, in which biological processes keep the partial pressure of $CO_2$ ($pCO_2$) much lower than in deeper waters. High-latitude areas, where deep water outcrops at the sea surface during winter, are an exception. The high $pCO_2$ in waters below about 300 m depth is attributed mainly to the downward transport of C, via gravitational settling of biogenic debris produced in the photic zone, and the slow vertical mixing rate of deep water. The models that have been used to estimate the uptake of $CO_2$ by the oceans incorporate these oceanic features in varying degrees and have been validated with observed distributions of tracers such as $^{222}Rn$, $^{14}C$, $^3H$, chlorofluorocarbons (CFCs), nutrient salts, and $O_2$. However, none of these tracers behaves exactly like $CO_2$. Furthermore, in all models the circulation is assumed to be in steady state, and in many of them changes in biological processes and the seasonal nature of C uptake are not included.

Measurements of $pCO_2$ in the surface waters and of total inorganic carbon ($TCO_2$) dissolved in the oceans have not yet led to a direct confirmation of the amount of fossil $CO_2$ removed from the atmosphere by the oceans (8), in part because the expected increases are small compared to the natural variation. For example, if half of the cumulative fossil fuel $CO_2$ emitted since 1850 were distributed uniformly in the upper 1000 m of the oceans, $TCO_2$ would have increased by only 1%.

Any geographical distribution of $CO_2$ sources and sinks is reflected in the spatial and temporal variations of $CO_2$ concentration patterns in the atmosphere. Numerical models of atmospheric transport can simulate these patterns; they thereby allow us to test hypotheses of the atmospheric $CO_2$ budget (9, 10). With the use of two-dimensional models (latitude, height) the observed concentration gradients in the atmospheric boundary layer can be inverted directly to yield the net surface source as a function of latitude and time (11). In this article, we use three-dimensional (3-D) transport fields to simulate the global distribution of $CO_2$ in response to specific assumptions about the strength and location of surface fluxes of $CO_2$. Global $CO_2$ budgets are constructed as linear combinations of separate sources and sinks, including new estimates for the oceanic fluxes. The mean annual meridional gradient observed from 1981 to 1987 is then compared with the model values, calculated as the corresponding linear combinations of the distributions generated separately for each source or sink, and thus used to select acceptable $CO_2$ source-sink scenarios.

## Atmospheric Observations

The Geophysical Monitoring for Climatic Change (GMCC) division of the National Oceanic and Atmospheric Administration (NOAA) has been collecting air samples in flasks for $CO_2$ analysis from more than 20 sites since 1980 (Table 1) (12). All flasks have been analyzed on the same nondispersive infrared analyzer in Boulder, Colorado, and referenced to the international manometric mole fraction scale (13) adopted for $CO_2$ monitoring. The seasonal cycles of $CO_2$ concentration observed at these sites have been used to estimate the seasonal net ecosystem production of the major terrestrial biomes of the world (10, 14). In this study we have used the average of the annual mean concentrations for 1981 to 1987 (Table 1 and Fig. 1). We have not used the data from all of the GMCC sites. Records from Niwot Ridge, Colorado, as well as Mauna Loa Observatory, Hawaii, were not used because mountainous terrain is not resolved well in the transport model. Specifically, we do not know what effective model height to assign to these sites. At some other sites, such as Cape Meares, Oregon, the data are too noisy to extract annual averages with sufficient confidence. The data yield a large-scale meridional gradient that corresponds closely to those obtained by other atmospheric $CO_2$ monitoring programs (14, 15).

## Oceanic Observations and $CO_2$ Flux Estimates

The observed $pCO_2$ difference ($\Delta pCO_2$) between the surface ocean and the atmosphere represents the thermodynamic driving potential for transfer of $CO_2$ gas across the sea surface and includes implicitly the combined effects of all the processes that influence the $CO_2$ distribution in the oceans and atmosphere. We have analyzed measurements of $\Delta pCO_2$ obtained from 1972 to 1989 (16) (Fig. 2). El Niño events, occurring irregularly every few years, reduce the $CO_2$ flux from the Eastern and Central Equatorial Pacific waters to virtually zero (17), but the equatorial measurements during the 1982–1983 and 1986–1987 events have been excluded. The oceans

were divided into 2° by 2° "pixels", and the mean $\Delta pCO_2$ value for each pixel was computed separately for two seasonal periods, January through April and July through October (18) (Fig. 3). To estimate the global distribution of $\Delta pCO_2$ during each of the two seasonal periods, we extrapolated the observed values into regions where observations were lacking using relations between water temperature and surface water $pCO_2$ observed in various oceanographic regimes (19).

The net $CO_2$ flux ($F$) across the air-sea interface was computed from

$$F = E\Delta pCO_2 = V_p S \Delta pCO_2 \qquad (1)$$

where $E$ is the gas transfer coefficient, $V_p$ is the gas transfer piston velocity, and $S$ is the solubility of $CO_2$ in seawater; $V_p$ depends on turbulence in both media and hence on the wind speed, $W$. Because the effects of temperature on $V_p$ and $S$ nearly cancel each other, $E$ is mainly a function of wind speed alone. Measurements of $V_p$ made under various wind regimes in the field and in wind tunnels show that $V_p$ is nearly zero for $W < 3$ m s$^{-1}$. They also show a wide range of variation (about a factor of 2) in $V_p$ for $W > 3$ m s$^{-1}$, the cause of which is not clearly understood. For $W > 3$ m s$^{-1}$ (the wind speed at 10 m above the sea surface), we adopted the relation (20)

$$E(\text{moles of } CO_2 \text{ m}^{-2} \text{ year}^{-1} \text{ } \mu\text{atm}^{-1}) = 0.016 [W(\text{m s}^{-1}) - 3] \qquad (2)$$

whereas $E$ is taken to be zero for $W < 3$ m s$^{-1}$. This relation yields $V_p$ values slightly lower than the upper limit of the wind-tunnel data (21). For comparison, Liss and Merlivat [(22), see also (23)], using results of experiments in wind tunnels and in the field (24), chose values about one half of our values. If their values are adopted, the resulting $CO_2$ transfer flux would be halved for a given value of $\Delta pCO_2$.

We calculated monthly values of $E$ for every 2° by 2° pixel using Eq. 2 and monthly climatological wind speeds compiled by Esbensen and Kushnir (25). The resulting annual mean global value for $E$

**Table 1.** Annual average concentrations of $CO_2$ above 300 ppmv (by volume) in dry air. Years for which the data quality was deemed insufficient have been omitted (dashes), and the lack of an ongoing program is indicated by blanks. For the calculation of the 1981 to 1987 average, all years were first normalized to 1987 by adding the globally averaged difference between 1987 and that year. In order to avoid biasing the global averages by the addition or omission of stations, the averages were calculated from third-degree polynomial curve fits to the available yearly data. The reported SD is a measure of the variability of the annual averages at each station after normalization to 1987.

| Name | Code | Location | 1981 | 1982 | 1983 | 1984 | 1985 | 1986 | 1987 | Average | SD |
|---|---|---|---|---|---|---|---|---|---|---|---|---|
| South Pole | SPO | 90°S | 38.5 | 39.3 | 40.7 | 42.2 | 43.6 | 44.6 | 46.8 | 46.59 | .17 |
| Halley Bay | HBA | 76°S, 26°W | | | | 41.2 | — | — | 45.0 | 47.2 | 47.11 | .23 |
| Palmer Station | PSA | 65°S, 64°W | | 39.5 | 40.9 | 42.7 | 43.9 | — | 47.0 | 46.91 | .13 |
| Cape Grim | CGO | 41°S, 145°E | | | | 42.5 | 43.7 | 44.6 | 46.5 | 46.54 | .11 |
| Amsterdam Island | AMS | 38°S, 78°E | | 39.3 | 41.1 | 42.4 | 43.9 | 45.0 | — | 46.82 | .20 |
| Samoa | SMO | 14°S, 171°W | 39.3 | 40.3 | 41.4 | 43.5 | 44.7 | 45.2 | 47.1 | 47.44 | .27 |
| Ascension Island | ASC | 8°S, 14°W | 39.8 | 40.7 | 42.6 | 43.9 | 45.0 | 45.8 | 48.1 | 48.07 | .33 |
| Seychelles | SEY | 5°S, 55°E | 40.2 | 40.5 | 41.1 | 44.1 | 45.2 | 46.1 | — | 47.93 | .41 |
| Christmas Island | CHR | 2°N, 157°W | | | | 44.7 | 45.9 | 46.3 | 48.5 | 48.56 | .32 |
| Guam | GMI | 13°N, 145°E | | 41.0 | 42.7 | 44.4 | 46.0 | — | — | 48.64 | .19 |
| Virgin Island | AVI | 18°N, 65°W | 40.3 | 40.9 | 42.0 | 43.4 | 45.4 | 46.4 | 48.2 | 48.13 | .28 |
| Cape Kumukahi | KUM | 20°N, 155°W | 40.6 | 41.2 | 42.6 | 44.3 | 45.6 | 46.5 | 48.5 | 48.52 | .14 |
| Key Biscayne | KEY | 26°N, 80°W | | | | 45.2 | 46.7 | 47.6 | 49.5 | 49.47 | .06 |
| Midway | MID | 28°N, 177°W | | | | | | 47.6 | 49.7 | 49.61 | .21 |
| Azores | AZR | 39°N, 27°W | | 41.2 | 43.0 | 44.5 | — | — | — | 48.77 | .21 |
| Shemya Island | SHM | 53°N, 174°E | | | | | | 48.9 | 50.0 | 50.39 | .52 |
| Cold Bay | CBA | 55°N, 163°W | 41.0 | 41.8 | 43.3 | 45.5 | 47.2 | 48.1 | 49.7 | 49.58 | .34 |
| Station "M" | STM | 66°N, 2°E | 41.8 | 42.1 | 43.1 | 45.5 | 46.5 | 48.2 | 48.8 | 49.49 | .42 |
| Point Barrow | BRW | 71°N, 157°W | 41.4 | 42.6 | 43.7 | 45.4 | 46.4 | 48.6 | 49.5 | 49.73 | .39 |
| Mould Bay | MBC | 76°N, 119°W | 41.8 | 42.4 | 43.6 | 45.6 | 46.7 | 48.6 | 49.8 | 49.85 | .28 |
| Alert | ALT | 83°N, 62°W | | | | | | 48.0 | 49.5 | 49.68 | .25 |
| Global average | | | 40.00 | 40.65 | 42.03 | 43.91 | 45.27 | 46.26 | 48.10 | 48.10 | |

**Table 2.** Estimates of sea-to-air $CO_2$ flux (Gt of C per year) based on the compilation of $\Delta pCO_2$ in microatmospheres in various oceans (Fig. 3) and transfer coefficients depending on wind speeds (see text). The seasonality of the $\Delta pCO_2$ and the winds has been taken into account. The north Indian Ocean is included in the equatorial oceans. Extrapolation of $\Delta pCO_2$ into ocean areas with no measurements is based on water temperatures (19).

| Ocean | Location | January to April | | July to October | | Annual mean | |
|---|---|---|---|---|---|---|---|
| | | $\Delta pCO_2$ | Flux | $\Delta pCO_2$ | Flux | $\Delta pCO_2$ | Flux |
| Atlantic subarctic | >50°N; 90°W to 20°E | −22 | −0.15 | −53 | −0.31 | −37 | −0.23 |
| Atlantic gyre | 15°N to 50°N; 90°W to 20°E | −29 | −0.58 | −1 | −0.02 | −15 | −0.30 |
| North Pacific | >15°N; 110°E to 90°W | −11 | −0.44 | 14 | 0.33 | 2 | −0.06 |
| Equatorial | 15°S to 15°N; 180°W to 180°E | 37 | 1.56 | 28 | 1.69 | 33 | 1.62 |
| Southern gyres | 50°S to 15°S; 180°W to 180°E | −9 | −1.46 | −25 | −3.31 | −17 | −2.39 |
| Antarctic | >50°S | −23 | −0.38 | −10 | −0.03 | −17 | −0.20 |
| Global | | 3 | −1.5 | −1 | −1.7 | 1 | −1.6 |

is 0.067 mol of $CO_2$ m$^{-2}$ year$^{-1}$ $\mu$atm$^{-1}$, which is consistent with the global mean $CO_2$ gas exchange rate of 20 ± 3 mol of $CO_2$ m$^{-2}$ year$^{-1}$, based on the distribution of $^{14}CO_2$ in the atmosphere and oceans (21) (hence Eq. 2 is "empirical"). The ocean fluxes were calculated from the seasonal $\Delta pCO_2$ maps (Fig. 3), Eq. 2, and the monthly climatological winds (25) (Table 2). This analysis gave a net $CO_2$ uptake of 1.6 Gt of C per year (1 Gt equals $10^{15}$ g), which corresponds to about 30% of the current rate of fossil fuel emissions.

A rigorous error analysis for this estimate cannot be made at this time, but most of the uncertainty is attributed to the sparsity of data in the South Pacific and South Indian oceans. In the North Pacific Ocean, where 26 trans-Pacific transects have been made during various seasons from 1984 to 1989, the uncertainty in $\Delta pCO_2$ due to the finite number of samples can be estimated. We removed an east-west transect data set (about 40 values) and computed pixel values using the remaining data (about 260 values for a seasonal map), after which we compared the values on the computed map with the removed transect. This comparison was made for three separate data sets, representing transects across the northern high-latitude areas in summer and winter, respectively, and one across the mid-latitudes during the winter. The root-mean-square difference between individual computed and measured values was 8 $\mu$atm, whereas the mean difference was about 1 $\mu$atm. This result suggests good consistency between the transects and only minor statistical sampling errors in this ocean basin, but does not address possible systematic errors. A systematic error of 1 $\mu$atm in the annual average $\Delta pCO_2$ would lead to a total flux error of about 0.07 Gt of C per year for the Arctic, North Atlantic, and North Pacific oceans combined. On the other hand, the same error in $\Delta pCO_2$ for the Southern Hemisphere oceans (south of 10°S) would cause an error in the net flux of about 0.15 Gt of C per year, mainly because of the greater area.

## Transport Modeling with Surface Sources and Sinks

We used a global 3-D atmospheric tracer model derived from the general circulation model (GCM) developed at Goddard Institute for Space Studies (GISS) of the National Aeronautics and Space Administration (26) to model the distribution of $CO_2$ in the atmosphere. The 3-D model is fully seasonal in terms of its transport and mixing characteristics (including parameterized diffusion) as well as in the sources and sinks of $CO_2$. The parent GCM has diurnal and seasonal cycles, and four hourly mass fluxes, as well as monthly averaged convective frequencies, were saved for the tracer transport model. In addition to producing realistic simulations of the large-scale features of the general circulation of the atmosphere, the GCM

transport fields have been validated by the simulation of inert tracers (27). For tracers with Northern Hemisphere mid-latitude sources, the interhemispheric exchange time has been adjusted via a subgrid diffusion parameterization to 1.0 year, intermediate between what is needed to match the observed north-south distributions of CFCs and $^{85}$Kr (exchange times of 0.9 and 1.1 years, respectively).

Two-dimensional models based on transport coefficients derived (28) from the GCM developed at the Geophysical Fluid Dynamics Laboratory (GFDL) have an interhemispheric exchange time for $^{85}$Kr (11) nearly identical to that in the GISS model. An independent 3-D transport model based on analyzed winds, as obtained by the European Center for Medium Range Weather Forecasting, together with a convective vertical mixing scheme, gives an interhemispheric transport time for $^{85}$Kr of 1.39 years (29). The calculated vertically and hemispherically averaged difference between the hemispheres for the fossil fuel source by the GISS model is the same as that derived for a simple atmospheric two-box model with an
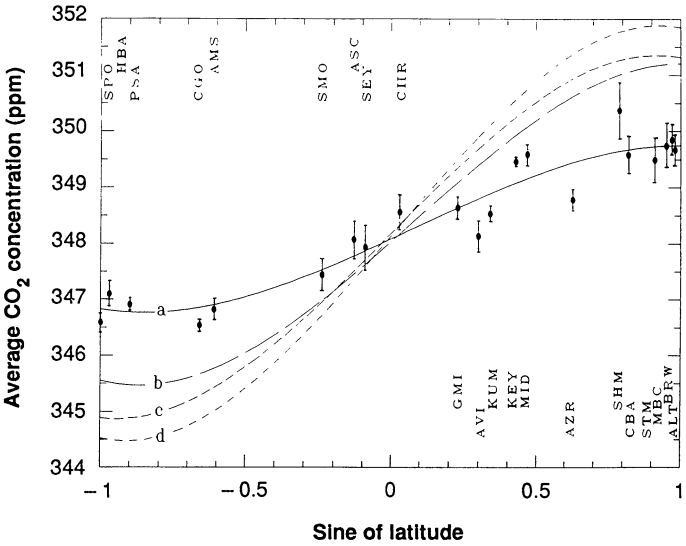


**Fig. 1.** Observed atmospheric $CO_2$ concentrations at the sites of the NOAA/GMCC flask network. The three-letter station codes are explained in Table 1. The error bars represent 1 SD of the annual averages at each site after adjustment to 1987. Curve (a) is a least-squares cubic polynomial fit to the data. The residual SD of the points with respect to the curve is 0.39 ppm. The concentration distributions at the NOAA/GMCC sites have also been calculated with the NASA/GISS GCM transport fields. Other curves are polynomial fits to the calculated $CO_2$ distributions (not shown) with fossil fuel emissions, seasonal vegetation (no net annual source or sink), tropical deforestation of 0.3 Gt of C per year, and three different cases of ocean uptake: (c), the compilation of $CO_2$ uptake based on the $\Delta pCO_2$ data (Table 2) and our empirical transfer coefficients; (b), $CO_2$ uptake based on the same $\Delta pCO_2$ map, but calculated with the Liss-Merlivat (22) relation for air-sea exchange; (d), an earlier estimate of ocean uptake (21) totaling 2.6 Gt of C per year.

interhemispheric exchange time of 1 year. Also, our two-dimensional model based on the transport derived from the GFDL GCM gave a virtually identical result.

The GISS transport model has been used to simulate the effects of seasonal $CO_2$ exchange with the terrestrial biosphere (30). The
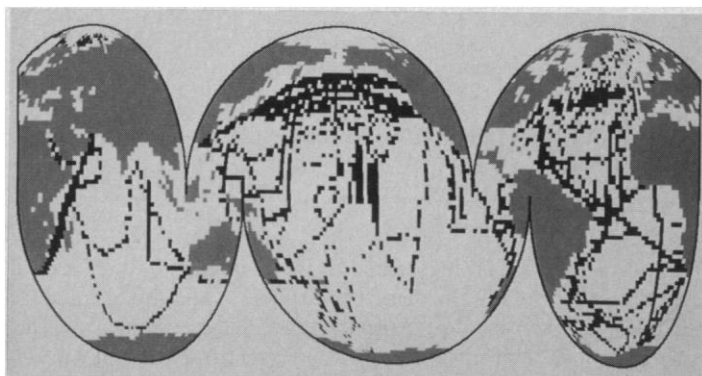


**Fig. 2.** The distribution of measurements of $\Delta pCO_2$ since 1972. Where observations were made quasi-continuously, the values have been averaged over 2° intervals in longitude and latitude, and each of these intervals is represented by a single dot on the map.

modeled annual oscillations are similar to those observed at the surface sampling sites, as well as to those found in aircraft data from Scandinavia, Japan, Australia (Fig. 4), and from various latitudes in the Northern Hemisphere at 500 and 700 mbar (31).

The covariance of seasonal transport and seasonal $CO_2$ sources and sinks may lead to annually averaged concentration differences between different sites, both in the model and in the atmosphere, even in the absence of net annual sources: If transport is less vigorous during the season when a surface region is a source rather than when it is a sink, a positive net annual concentration anomaly will result. With purely seasonal annually balanced sources, the GISS 3-D model calculates annual mean concentrations for the GMCC sites in the Northern Hemisphere that are on average 0.25 ppm higher than for the sites in the Southern Hemisphere, whereas a 2-D model (11) gives a difference of only 0.05 ppm. There are no independent tracers to validate this aspect of the models. The most important reason for the difference is the summer-to-winter variability of vertical convective mixing at high latitudes. The greater vertical stability in winter would tend to keep the respired $CO_2$ closer to the ground, which would result in higher annual average surface $CO_2$ concentrations in the Northern Hemisphere.

We used the 3-D model to test hypotheses about global $CO_2$ budgets, constructed as linear combinations of separate source-sink
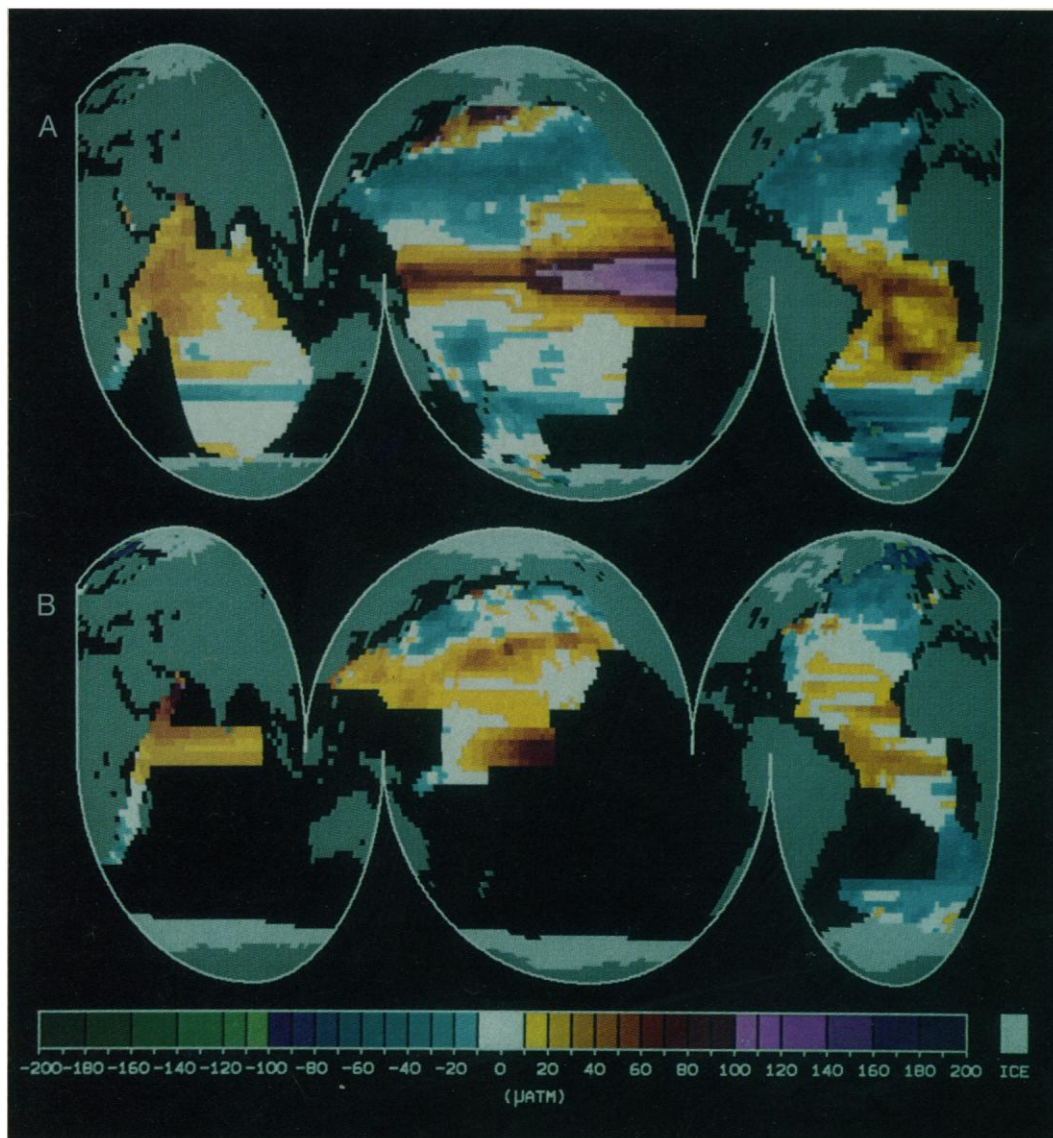


**Fig. 3.** Observed $\Delta pCO_2$ (in microatmospheres) between surface waters of the oceans and the atmosphere during two seasonal periods, (**A**) January through April and (**B**) July through October. These maps have been compiled from direct observations made since 1972 (Fig. 2) and represent the mean distributions during the past 16 years, excluding the El Niño conditions in the equatorial Pacific. Areas of ice cover are indicated in light gray.

patterns. We first calculated the $CO_2$ distribution for each source separately by running the model with that source for 3 years, during which the annual average concentration gradients became stabilized. The $CO_2$ distributions computed for the last year of the simulations were used in our analyses. As a sign convention, fluxes into the atmosphere (sources) are positive, fluxes from the atmosphere (sinks) negative. For any hypothesized global budget to be acceptable, it must satisfy two observational criteria: first, the total atmospheric inventory must increase by 3.0 Gt of C per year (corresponding to 1.4 ppm per year), and second, the corresponding linear combination of the modeled response distributions must reasonably resemble the observed atmospheric concentration differences at the stations.

The residuals, departures of the modeled annual average $CO_2$ concentrations from those observed at the GMCC sites, were fit with a third-order polynomial and with a straight line. In this way we were looking for consistent patterns of disagreement between the model and the data, because we did not want to adjust sources solely on the basis of discrepancies at single points. A source scenario is considered not plausible if the slope of the linear fit or any structure in the polynomial fit is statistically significant. The linear slope constraint requires that the strength of extratropical sources and sinks in the Northern relative to those in the Southern Hemisphere be determined to within about 0.2 Gt of C per year.

## A Test of Some Current Views of the $CO_2$ Budget

The geographical distribution of fossil fuel combustion (32) was combined with several global compilations of $CO_2$ exchange with the oceans and the terrestrial biosphere. The fossil fuel source was 5.3 Gt of C per year, typical of that from 1980 to 1987, when the global fossil fuel consumption remained fairly constant. Seasonal exchange with the terrestrial biosphere (30) was included although it does not affect the global budget. Tropical deforestation was assumed to be a source of 0.3 Gt of C per year, at the low end of the release estimates. Three ocean estimates were tested. In the first, our ocean data analysis presented above (Table 2) was used, and in this case an additional $CO_2$ sink of 1 Gt of C per year is required to balance the budget because the observed atmospheric increase is 3.0 Gt of C per year. In the second, the $\Delta pCO_2$ values were combined with the air-sea transfer coefficients proposed by Liss and Merlivat

(22); this scenario results in a total ocean uptake of only 0.8 Gt of C per year, in which case an extra sink of 1.8 Gt of C per year is required. In the third, we set the global net ocean sink to 2.6 Gt of C per year (21), thus balancing the budget.

The simulated difference in atmospheric $CO_2$ between the north and south poles resulting exclusively from fossil fuel combustion without any $CO_2$ sinks was 4.4 ppm. The uncertainty in the $CO_2$ production from fossil fuel combustion is estimated to be between 6 and 10% (33), and about 5% (34) of the fuel carbon is only partially oxidized to CO during combustion. This CO is oxidized in the atmosphere by reaction with OH radicals, which are concentrated at lower latitudes. This effect is neglected in the scenario, so that the calculated pole-to-pole gradient for fossil fuel combustion alone could be between 3.8 to 4.6 ppm. The seasonal terrestrial $CO_2$ exchange and tropical deforestation together are calculated to add another 0.6 ppm to the pole-to-pole gradient. The inclusion of the oceanic sink, acting strongly in the Southern Hemisphere, resulted in a meridional gradient between both poles of 5.7 to 7.3 ppm, depending on the ocean scenario. These values are contradicted in all
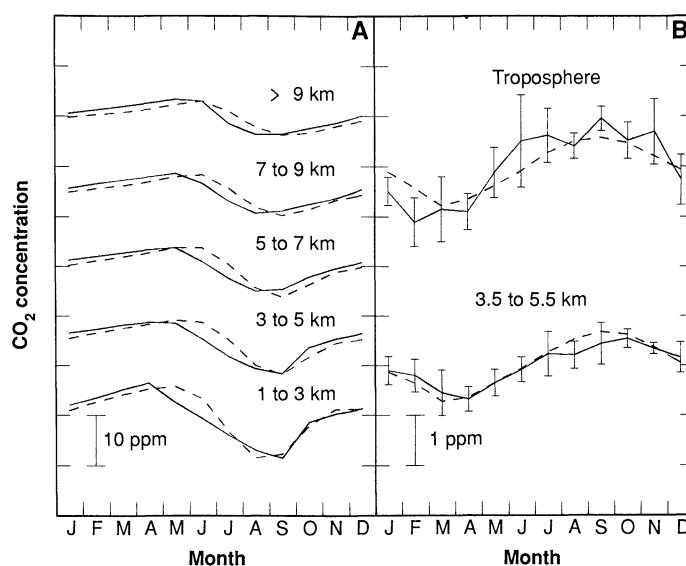


**Fig. 4.** Comparison of the observed (31) (solid line) and GISS-model calculated (30) (dashed line) annual cycle of $CO_2$ at different altitudes in the troposphere over (**A**) Scandinavia (67°N, 20°E) and (**B**) Bass Strait (40°S, 150°E).

**Table 3.** Four modeled scenarios of the global atmospheric cycle. Fluxes are in units of gigatons of C per year and $\Delta pCO_2$ is in microatmospheres. The terrestrial sources and sinks correspond to the basis functions: (i) tropical deforestation, (ii) carbon sequestering by temperate ecosystems, and (iii) $CO_2$ fertilization (see text). Fossil fuel combustion and the seasonality of the terrestrial biosphere is included in all cases. After fluxes to and from the terrestrial biosphere have been postulated, uptake by the oceans is adjusted to minimize the SD (in parts per million, last line) of the residual differences between the observed and calculated atmospheric $CO_2$ concentrations. The required annual average $\Delta pCO_2$ is estimated for ocean basins with empirical air-sea gas transfer coefficients.

| Source or sink | Scenario 1, flux $\Delta pCO_2$ | | Scenario 2, flux $\Delta pCO_2$ | | Scenario 3, flux $\Delta pCO_2$ | | Scenario 4, flux $\Delta pCO_2$ | |
|---|---|---|---|---|---|---|---|---|
| Tropical deforestation | 0.3 | | 0.3 | | 2.0 | | 2.0 | |
| Temperate ecosystem uptake | 0.0 | | 0.0 | | 0.0 | | −1.0 | |
| $CO_2$ fertilization | 0.0 | | −1.0 | | 0.0 | | 0.0 | |
| Total terrestrial | 0.3 | | −0.7 | | 2.0 | | 1.0 | |
| North Atlantic (>50°N) | −0.7 | −72 | −0.5 | −52 | −0.7 | −72 | −0.5 | −52 |
| North Atlantic gyre (15° to 50°N) | −1.0 | −52 | −0.8 | −42 | −1.4 | −73 | −1.0 | −52 |
| North Pacific gyre (>15°N) | −1.0 | −24 | −0.7 | −17 | −1.4 | −34 | −1.0 | −24 |
| Equatorial (15°S to 15°N) | 1.0 | 22 | 1.0 | 22 | 1.0 | 22 | 1.0 | 22 |
| Combined southern gyres (15° to 50°S) | −1.4 | −14 | −1.1 | −11 | −2.3 | −23 | −2.3 | −23 |
| Antarctic (>50°S) | 0.5 | 9 | 0.5 | 9 | 0.5 | 9 | 0.5 | 9 |
| Total oceans | −2.6 | | −1.6 | | −4.3 | | −3.3 | |
| SD of residuals | 0.25 | | 0.24 | | 0.26 | | 0.25 | |

cases by the atmospheric data (Fig. 1) which exhibit a difference of only 3.0 ppm. What is wrong? In order to decrease the modeled gradient due to the fossil fuel source alone, either the extratropical net sink in the Northern Hemisphere must be larger than in the Southern Hemisphere, or there is a serious problem with the simulations of atmospheric transport in the GCM.

The annually averaged interhemispheric transport in the GCM is constrained by the $^{85}$Kr and CFC calibrations, and we estimate that this part of the uncertainty in the calculated pole-to-pole concentration gradient is 10% or less. The behavior of the seasonal cycle of $CO_2$ as a function of altitude is well represented by the model (30, 31) in the few places where data are available. Inverse calculations with two-dimensional transport models (11) have similarly shown that the sink of $CO_2$ needs to be substantially larger in the Northern Hemisphere than in the Southern Hemisphere. As the peak-to-trough amplitude of the mean Northern Hemisphere $CO_2$ annual cycle is about 8 ppm, it is unlikely that covariation of this seasonal source and seasonal transport could produce a north-south counter-gradient as large as 3 to 4 ppm to allow the southern oceans to be the dominant sink of fossil fuel $CO_2$. Therefore, the presence of a large sink of C in the Northern Hemisphere is a more likely cause for the discrepancy than problems with the model transport.



**Fig. 5.** Results of model calculations (scenario 1, Table 3) of the atmospheric $CO_2$ concentrations at the GMCC sites (squares and dashed curve) are compared with the observed concentrations (circles and solid curve). All values are relative to the global mean. The curves are least-squares cubic polynomial fits; the differences between the curves are not statistically significant.

## $CO_2$ Patterns from Single Source Regions

Before we discuss $CO_2$ source-sink scenarios, that is, linear combinations of sources and sinks that satisfy the two constraints, we describe the series of "basis" sources and simulations of the corresponding $CO_2$ response distributions made with the 3-D model. Atmospheric $CO_2$ patterns were calculated separately for eight oceanic source regions: the equatorial oceans between 15°N and 15°S, the North Pacific gyre north of 15°N, the North Atlantic north of 50°N, the North Atlantic gyre between 15°N and 50°N, the South Atlantic, South Pacific and Indian ocean gyres each between 15°S and 50°S, and the Antarctic Ocean south of 50°S. In each of these cases the source was assumed, as a first approximation, to be constant in time and uniformly distributed in its respective area. The resulting concentration patterns were as expected: for example, if there is a $CO_2$ source of 1 Gt of C per year in the North Atlantic gyre, the $CO_2$ concentrations at AZR, KEY, and AVI (Table 1) stand out from values at Pacific stations at similar latitudes by about 0.6 ppm. To reduce the number of independent variables, we assumed that the fluxes were proportional to area in the three southern ocean gyres, and we held the equatorial ocean source fixed at 1 Gt of C per year (21). We then had five ocean areas left as variables, the North Atlantic, the two north temperate gyres, the combined southern gyres, and the waters around Antarctica.

We considered four "basis functions" of net annual $CO_2$ exchange with the terrestrial biosphere: (i) net release due to deforestation in the tropics (3); (ii) C sequestering by temperate ecosystems; (iii) storage of C by high latitude boreal ecosystems; (iv) and a hypothetical sink due to enhanced net photosynthesis, which is referred to as $CO_2$ fertilization. For the second basis function, the C sink was uniformly distributed among locations associated with cold-deciduous forests (13 × 10$^6$ km$^2$); similarly for the third, the sink was distributed among evergreen needle-leaved forests and woodlands (12 × 10$^6$ km$^2$) and tundra (7 × 10$^6$ km$^2$). Carbon sequestering in these regions may be through processes such as reforestation (35) or accumulation of organic matter in soils. For the fourth sink, we assumed that the net fertilization is proportional to net primary productivity (NPP); thus, this sink is intense in tropical regions because of their high NPP (36). A global fertilization effect of 1 Gt of C per year, for example, would represent an increase of only 2%
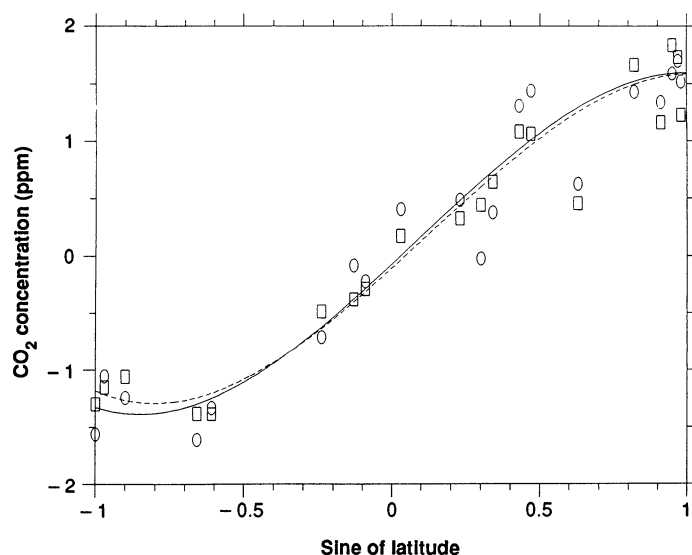
of NPP if ecosystem respiration remained the same. This amount is easily within the uncertainties of global NPP estimates (36).

In the simulations we took into account the covariance of the annually balanced seasonal $CO_2$ exchange (30) with terrestrial plants (no net annual flux) and the seasonality of the transport as a separate "basis" source scenario. The inclusion of this scenario significantly improved the comparison between the modeled and the observed concentrations with respect to the longitudinal variability.

## Adjustment of Oceanic Uptake to Terrestrial Scenarios

After we specified a priori certain combinations of gain and loss of C on the continents, uptake by the oceans was adjusted in each case until satisfactory agreement with the atmospheric observations was obtained. The four scenarios (Table 3 and Fig. 5) all fit the atmospheric observations equally well; these data by themselves do not permit us to determine whether any one is more likely. In fitting the data, we could, to a limited extent, trade off uptake of C by terrestrial ecosystems against uptake by the oceans, for example, boreal forest and tundra ecosystems against the North Atlantic. Monitoring techniques need to be developed for and extended to the continental interiors to preclude such freedom in modeling and to pinpoint the source-sink distributions much more definitively.

The disagreement with Table 2 for the uptake of $CO_2$ by the southern oceans stems mainly from the limited number of $\Delta pCO_2$ observations in the high-latitude waters near Antarctica. The atmospheric data seem to indicate that there is a $CO_2$ source in the waters around Antarctica. This estimate for the Antarctic waters rests on the concentration difference between HBA and PSA on the one hand and SPO, CGO, and AMS on the other hand (Fig. 1). Recent oceanographic measurements (37) appear to have provided some confirmation for the presence of a $CO_2$ source (Fig. 3B).

Atmospheric $CO_2$ concentrations at AVI, KEY, and AZR (Table 1) in the Atlantic relative to KUM and MID in the Pacific suggest that the average $pCO_2$ of the North Pacific should be higher than the North Atlantic. The $\Delta pCO_2$ observations confirm this (Fig. 3).

All of the scenarios (Table 3), however, are equally unrealistic because the mean annual $\Delta pCO_2$ required for the Northern Hemisphere oceans is much greater than observed (Fig. 3). The discrepancy is much larger than can be explained by the uncertainty in the $\Delta pCO_2$ data. Use of the gas exchange rates of Liss and Merlivat (22) would double this discrepancy.

## Adjustment of Terrestrial Exchange to Observed $\Delta pCO_2$

Because of the conflict of the $\Delta pCO_2$ required by the foregoing scenarios and the observed $\Delta pCO_2$ of the northern oceans, we constructed several scenarios in which $CO_2$ fluxes in better known oceanic regions were kept fixed (with linear interpolation for the intervening months), namely uptake by the northern oceans and $CO_2$ outgassing from the equatorial oceans (Table 2). Exchange with the terrestrial ecosystems and with the southern oceans was varied to produce agreement with the atmospheric data.

Several types of scenarios (four are presented in Table 4) all agreed about equally well with the atmospheric data. The constraint of the observed north-south gradient imposes two important common features. First, a large terrestrial sink at northern temperate latitudes is necessary, and second, total $CO_2$ uptake by the oceans is considerably less than uptake by terrestrial systems. The total terrestrial sink at high northern and temperate latitudes (including its share of the global $CO_2$ fertilization) varies between 2.0 and 2.7 Gt of C per year in the four scenarios. The sum of the temperate and high-latitude sources and sinks is tightly constrained, but the two can be traded off against one another to some extent. However, a large temperate sink requires a smaller high-latitude source to prevent the modeled $CO_2$ concentration at arctic sites from becoming too low.

The following scenarios were unsuccessful: The additional absorption of more than a few tenths of a gigaton of C by high latitude ecosystems or the Arctic Ocean resulted in predicted concentrations for the five northernmost stations that were too low. Balancing the global budget by uptake via $CO_2$ fertilization proportional to NPP (and no tropical deforestation) left the concentrations at equatorial latitudes too low; half of the NPP takes place in the tropics, so that the area would in that case act as a net sink for $CO_2$.

The modeled $CO_2$ gradients are not very sensitive to the magnitude of tropical deforestation because the GMCC sites are remote from deforestation activities and the released $CO_2$ is dispersed rapidly via vigorous vertical mixing. If the release of $CO_2$ from tropical forest destruction is balanced by the fertilization effect, half of the extra $CO_2$ is taken up in the tropics themselves, and thus smaller amounts of carbon uptake are required at temperate latitudes in both hemispheres. A large amount of tropical deforestation (scenario 8, Table 4) can only be accommodated if $CO_2$ fertilization is a strong sink, so that the modeled tropical $CO_2$ concentrations do not become significantly larger than those observed.

We have not included in the simulations the atmospheric oxidation of CO, which produces a total of $0.85 \pm 0.25$ Gt of C per year of $CO_2$ (34). Simulations with a two-dimensional model of a latitudinal and seasonal distribution of CO oxidation totaling 1 Gt of C per year globally (38) suggest that a broad maximum in $CO_2$ concentrations forms at 30°N that decreases by 0.3 ppm toward the South Pole and by 0.15 ppm toward the North Pole. The inclusion of this process would have reinforced the need for a northern mid-latitude sink. As a related problem, a small part of the terrestrial sink for $CO_2$ that we infer will not contribute to C storage on the land because C is recycled by the biosphere into reduced volatile compounds that are oxidized, often via CO, to $CO_2$ in the atmosphere.

## Conclusions

From 1981 to 1987 atmospheric $CO_2$ increased at an average rate of 3.0 Gt of C per year. The release of $CO_2$ from fossil fuel burning (5.3 Gt of C per year) and land use modification (0.4 to 2.6 Gt of C per year) is being partially balanced by the uptake of $CO_2$ by the oceans and by terrestrial ecosystems. Observations and simulations of the meridional gradient of $CO_2$ in the atmosphere suggest that these sinks are larger in the Northern Hemisphere than in the Southern Hemisphere.

The atmospheric gradient constrains the combined uptake by the southern ocean gyres and Antarctic waters to be from 0.6 to 1.4 Gt of C per year. In consideration of the large data base of seasonal $\Delta pCO_2$ measurements in the surface waters of the Northern Hemisphere, the uncertainties in $\Delta pCO_2$ are most likely not large enough to accommodate the values of C removal required without a large

**Table 4.** Four modeled scenarios of the global atmospheric C cycle in which uptake by the northern and equatorial oceans is held fixed. Fluxes are in units of Gt of C per year. Equatorial ocean outgassing is lower than in Table 2 by 0.32 Gt of C per year to take into account El Niño episodes occurring about once every 4 years. After the rate of tropical deforestation has been postulated, $CO_2$ exchange with terrestrial ecosystems and the southern oceans is varied (indicated by asterisk) to produce agreement with the atmospheric observations. The estimates of uptake by the oceans are based on observed seasonal $\Delta pCO_2$ values, monthly climatological winds and two sets of air-sea gas transfer coefficients, our empirical relation (Emp), and the Liss-Merlivat (22) relation (LM). In the latter case the equatorial oceanic source is smaller, so that less uptake is required at temperate latitudes in both hemispheres to balance the budget.

| Source or sink | Scenario 5 | | Scenario 6 | | Scenario 7 | | Scenario 8 | |
| --- | --- | --- | --- | --- | --- | --- | --- | --- |
| | Emp | LM | Emp | LM | Emp | LM | Emp | LM |
| Tropical deforestation | 0.0 | 0.0 | 1.0 | 1.0 | 1.0 | 1.0 | 2.5 | 2.5 |
| $CO_2$ fertilization* | 0.0 | 0.0 | 0.0 | 0.0 | -1.0 | -1.0 | -3.0 | -3.0 |
| Temperate uptake* | -2.0 | -2.0 | -3.0 | -2.9 | -2.3 | -2.0 | -1.9 | -1.9 |
| Boreal source* | 0.0 | 0.0 | 0.4 | 0.4 | 0.4 | 0.2 | 0.7 | 0.7 |
| Total terrestrial | -2.0 | -2.0 | -1.6 | -1.5 | -1.9 | -1.8 | -1.7 | -1.7 |
| Arctic and sub-arctic (>50°N) | -0.23 | -0.12 | -0.23 | -0.12 | -0.23 | -0.12 | -0.23 | -0.12 |
| Combined northern gyres (15°N to 50°N) | -0.36 | -0.18 | -0.36 | -0.18 | -0.36 | -0.18 | -0.36 | -0.18 |
| Equatorial (15°S to 15°N) | 1.30 | 0.65 | 1.30 | 0.65 | 1.30 | 0.65 | 1.30 | 0.65 |
| Combined southern gyres* (50°S to 50°S) | -1.5 | -1.1 | -1.9 | -1.6 | -1.6 | -1.3 | -1.8 | -1.4 |
| Antarctic (>50°S) | 0.5 | 0.5 | 0.5 | 0.5 | 0.5 | 0.5 | 0.5 | 0.5 |
| Total oceans | -0.3 | -0.3 | -0.7 | -0.8 | -0.4 | -0.5 | -0.6 | -0.6 |
| SD of residuals (ppm) | 0.26 | 0.28 | 0.27 | 0.29 | 0.27 | 0.28 | 0.28 | 0.29 |

terrestrial sink. We infer that the global ocean sink is at most 1 Gt of C per year. Our analysis thus suggests that there must be a terrestrial sink at temperate latitudes to balance the carbon budget and to match the north-south gradient of atmospheric $CO_2$. The mechanism of this C sink is unknown; its magnitude appears to be as large as 2.0 to 3.4 Gt of C per year, depending on the sources in the tropical and the boreal and tundra regions.

The global C cycle is not well understood. Unraveling the contemporary $CO_2$ cycle and the development of future mitigation strategies requires a concerted measurement program to determine the seasonal fluxes of $CO_2$ between the atmosphere, land, and oceans. Our hypothesis suggests that annually averaged $\Delta pCO_2$ values in the combined southern oceans are small negative values. Collection of data on air-sea exchange of $CO_2$ in these areas in all seasons should be given high priority. Understanding the role of the land in the C budget must include a reanalysis of the contribution of mid-latitude reforestation as well as studies of the feedbacks between ecosystem functioning, climate, and atmospheric composition.

The atmosphere integrates the fluxes from all sources and sinks. It thus contains the large-scale signatures of $CO_2$ source areas that are often highly variable, and therefore hard to measure, on smaller scales. Data from the present international network of $CO_2$ monitoring sites, located almost exclusively in oceanic areas, cannot be used to resolve longitudinal gradients, and thus identification of the important source-sink areas is currently difficult. In addition, high-precision measurements of the large-scale variations of $^{13}C/^{12}C$ ratios in $CO_2$ and the concentration of atmospheric $O_2$ are needed to untangle the contributions of the land and oceans.

## REFERENCES AND NOTES

1. R. E. Dickinson and R. J. Cicerone, *Nature* **319**, 109 (1986); V. Ramanathan, *Science* **240**, 293 (1988); J. Hansen *et al.*, *J. Geophys. Res.* **93**, 9341 (1988).
2. G. Marland *et al.*, *Estimates of $CO_2$ Emissions from Fossil Fuel Burning and Cement Manufacturing* (Oak Ridge Natl. Lab. Rep. ORNL/CDIAC-25, National Technical Information Service, Springfield, VA, 1989).
3. B. Bolin, *Science* **196**, 613 (1977); G. M. Woodwell *et al.*, *ibid.* **199**, 141 (1978); R. P. Detwiler and C. A. S. Hall, *ibid.* **239**, 42 (1988).
4. R. A. Houghton *et al.*, *Tellus* **39B**, 122 (1987).
5. E. R. Lemon, Ed., *$CO_2$ and Plants* (Am. Assoc. Adv. Sci. Select. Symp. Ser. 84, Westview, Boulder, 1983); B. R. Strain and J. D. Cure, Eds., *Direct Effects of Increasing Carbon Dioxide on Vegetation* (U.S. Dept. Energy Rep. DOE/ER-0238, National Technical Information Service, Springfield, VA, 1985); W. R. Emanuel, G. E. G. Killough, J. S. Olson, in *Carbon Cycle Modelling*, B. Bolin, Ed. (Wiley, New York, 1981), pp. 335–354; L. H. Allen *et al.*, *Glob. Biogeochem. Cyc.* **1**, 1 (1987).
6. W. S. Broecker, T. Takahashi, H. J. Simpson, T.-H. Peng, *Science* **206**, 409 (1979).
7. C. D. Keeling, in *Chemistry of the Lower Atmosphere*, S. I. Rasool, Ed. (Plenum, New York, 1973), pp. 251–329; H. Oeschger, U. Siegenthaler, U. Schotterer, A. Gugelmann, *Tellus* **27**, 168 (1975); R. Bacastow and A. Bjorkstrom, in *Carbon Cycle Modelling*, B. Bolin, Ed. (Wiley, New York, 1981) pp. 29–80; T.-H. Peng, *Radiocarbon* **28**, 363 (1986); E. Maier-Reimer and K. Hasselmann, *Climate Dyn.* **2**, 63 (1987); J. R. Toggweiler, K. Dixon, K. Bryan, *J. Geophys. Res.* **94**, 8217 (1989); *ibid.*, p. 8243 (1989).
8. J. R. Trabalka, Ed., *Atmospheric Carbon Dioxide and the Global Carbon Cycle* (U.S. Dept Energy Rep. DOE/ER-0239, National Technical Information Service, Springfield, VA, 1985).
9. G. I. Pearman and P. Hyson, *J. Geophys. Res.* **85**, 4468 (1980).
10. I. Fung *et al.*, *ibid.* **88**, 1281 (1983).
11. I. G. Enting and J. V. Mansbridge, *Tellus* **41B**, 111 (1989); P. P. Tans, T. J. Conway, T. Nakasawa, *J. Geophys. Res.* **94**, 5151 (1989).
12. W. D. Komhyr *et al.*, *J. Geophys. Res.* **90**, 5567 (1985); T. J. Conway *et al.*, *Tellus* **40B**, 81 (1988). Since 1983 the flask samples have also been analyzed for methane [L. P. Steele *et al.*, *J Atmos. Chem.* **5**, 125 (1987)].
13. All values are relative to the World Meteorological Organization X85 scale for $CO_2$ [P. R. Guenther and C. D. Keeling, *Scripps Reference Gas Calibration System for $CO_2$-in-Air Standards: Revision of 1985* (Scripps Institute of Oceanography, La Jolla, CA, 1985)].
14. G. I. Pearman and P. Hyson, *J Atmos. Chem.* **4**, 81 (1986).
15. C. D. Keeling and M. Heimann, *J Geophys. Res.* **91**, 7782 (1986).
16. The data base used consists mainly of the measurements obtained by the Lamont-Doherty Geological Observatory. This has been supplemented by data in the North Atlantic by M. Roos and G. Gravenhorst [*J. Geophys. Res.* **89**, 8181 (1984)]; in the equatorial Atlantic by C. Andrie, C. Oudot, C. Genthon, and L. Merlivat [*ibid.* **91**, 11,741 (1984)]; and in the North and South Pacific oceans and the eastern Indian Ocean by R. Gammon [personal communication]. When measurements were made continuously with a flow-through equilibrator, a mean value for each 2°

17. R. A. Feely *et al.*, *J. Geophys. Res.* **92**, 6545 (1987).
18. The measured values were weighted inversely proportional to the square of the distance from the center of the pixel, and those obtained in different years were weighted equally; $\Delta pCO_2$ values in pixels with no measurements, but surrounded by pixels with measured $\Delta pCO_2$ values, were estimated in gyre areas by linear interpolation in both latitude and longitude. In the equatorial zone, where currents are dominated by zonal flows, the value interpolated along the same latitude was used.
19. To extrapolate $\Delta pCO_2$ values into areas where measurements were not available (black areas in Fig. 3), the seawater $pCO_2$ was assumed to be a function of temperature alone. The following temperature coefficients were determined on the basis of the measurements made during various seasons and are assumed to be independent of seasons: 1.6% °$C^{-1}$ in the western North Atlantic (10°N to 40°N) and the south Indian Oceans (10°S to 34°S); 2.3% °$C^{-1}$ in the South Atlantic (10°S to 34°S) and South Pacific (10°S to 34°S); 4.3% °$C^{-1}$ in the eastern North Pacific (10°N to 34°N, 84°W to 154°W); 1.2% °$C^{-1}$ in the Southern Ocean (34°S to 62°S). The climatological sea surface temperature data compiled by S. Levitus [*Climatological Atlas of the World Ocean, NOAA Prof. Pap. 13*, pp. 173 (1982)] were used. In the Pacific coastal areas along the Central and South Americas, where high $\Delta pCO_2$ values occur because of upwelling of deep water, the $\Delta pCO_2$ data obtained outside the two seasonal periods have been used with the assumption that the values do not change seasonally.
20. T.-H. Peng and T. Takahashi, in *Biogeochemistry of $CO_2$ and the Greenhouse Effect*, M. P. Farrell, Ed. (Am. Chem. Soc. Symp., CRC/Lewis, Boca Raton, FL, in press).
21. W. S. Broecker *et al.*, *J. Geophys. Res.* **91**, 10517 (1986); T. Takahashi *et al.*, *Seasonal and Geographic Variability of Carbon Dioxide Sink/Source in the Oceanic Areas* (Tech. Rep. for Contr. MRETTA 19X-89675C, Lamont-Doherty Geological Observatory, Palisades, NY, 1986); H.-C. Broecker, J. Petermann, W. Siems, *J. Mar. Res.* **36**, 595 (1978).
22. P. Liss and L. Merlivat, in *The Role of Air-Sea Exchange in Geochemical Cycling*, P. Buat-Menard, Ed. (Adv. Sci. Inst. Ser. 185, Reidel, Hingham, 1986), pp. 113–127. Their formulation of the wind-speed-dependent gas exchange is
$$E = 0.00048W \text{ for } 0 \le W \le 3.6 \text{ m s}^{-1}$$
$$E = 0.0083(W - 3.39) \text{ for } 3.6 \le W \le 13 \text{ m s}^{-1}$$
$$E = 0.017(W - 8.36) \text{ for } W \ge 13 \text{ m s}^{-1}$$
23. J. Etcheto and L. Merlivat, *J. Geophys. Res.* **93**, 15669 (1988). If high-frequency wind speed data are used with the Liss-Merlivat relation, the seasonal mean gas transfer rate would increase at high latitudes by about 25% in the northern oceans and by 50% in the southern oceans because of the nonlinear character of the relation [J. Etcheto and L. Merlivat, *Adv. Space Res.* **9**, 141 (1989)].
24. R. Wanninkhof, J. R. Ledwell, W. S. Broecker, *Science* **227**, 1224 (1985); R. Wanninkhof, J. R. Ledwell, W. S. Broecker, M. Hamilton, *J. Geophys. Res.* **92**, 14,567 (1987).
25. S. K. Esbensen and Y. Kushnir, *The Heat Budget of the Global Oceans: An Atlas Based on Estimates from the Surface Marine Observations* (Clim. Res. Inst. Rep. 29, Oregon State University, Corvallis, OR, 1981).
26. G. L. Russell and J. A. Lerner, *J. Appl. Meteor.* **20**, 1483 (1981); J. G. Hansen *et al.*, *Mon. Weather Rev.* **111**, 609 (1983). The version used in this study and in (30) has 4° by 5° resolution and has improved simulation of the higher moment statistics of the general circulation.
27. M. Prather, M. McElroy, S. Wofsy, G. Russell, D. Rind, *J. Geophys. Res.* **92**, 6579 (1987); D. J. Jacob, M. J. Prather, S. C. Wofsy, M. B. McElroy, *ibid.*, p. 6614.
28. R. A. Plumb and J. D. Mahlman, *J. Atmos. Sci.* **44**, 298 (1987).
29. M. Heimann and C. D. Keeling, in *Aspects of Climate Variability in the Pacific and the Western Americas*, D. H. Peterson, Ed. (Geophysical Monograph 55, American Geophysical Union, Washington, DC, 1989).
30. I. Y. Fung, C. J. Tucker, K. C. Prentice, *J. Geophys. Res.* **92**, 2999 (1987).
31. We have made comparisons with aircraft data from C. D. Keeling, T. B. Harris, E. M. Wilkins, *J. Geophys. Res.* **73**, 4511 (1968); B. Bolin and W. Bischof, *Tellus* **22**, 431 (1970); G. I. Pearman and D. J. Beardsmore, *ibid.* **36B**, 1 (1984); M. Tanaka, T. Nakasawa, S. Aoki, *ibid.* **39B**, 3 (1987).
32. G. Marland, R. M. Rotty, R. L. Treat, *Tellus* **37B**, 243 (1985).
33. G. Marland and R. M. Rotty, *ibid.* **36B**, 232 (1984).
34. W. Seiler and R. Conrad, in *The Geophysiology of Amazonia*, R. E. Dickinson, Ed. (Wiley, New York, 1987), pp. 133–160.
35. T. V. Armentano and C. W. Ralston, *Can. J. Forest. Res.* **10**, 53 (1980); W. C. Johnson and D. M. Sharpe, *ibid.* **13**, 372 (1983).
36. H. Lieth, in *Primary Productivity of the Biosphere*, H. Lieth and R. Whittaker, Eds. (Ecolog. Stud. 14, Springer, New York, 1975), pp 203–213.
37. H. Inoue and Y. Sugimura, *Tellus* **40B**, 308 (1988).
38. P. Logan, personal communication.